Modelling the Trojan Asteroids

Christopher Gallagher *University of Cambridge*

April 22, 2020

Trojan asteroids are v important. I'm going to make that paragraph a little longer to fill out the space in case this is forming some kind of error. i really hope this is long enough.

1 Introduction

The Jupiter trojans, commonly known as the Trojan asteroids, are two large groups of asteroids that share the planet Jupiter's orbit around the Sun in a 1:1 orbit resonance. These two groups are called the Greeks and the Trojans, named after opposing sides in the mythological Trojan war, and lead/trail Jupiter respectively in its orbit. They correspond to Jupiter's two stable Lagrange points: L_4, lying 60° ahead of the planet in its orbit, and L_5, 60° behind, with asteroids distributed in two elongated, curved regions around these Lagrangian points.

The first Jupiter trojan, 588 Achilles, was discovered in 1906 by the German astronomer Max Wolf [1], and a total of 7642 Jupiter trojans have been found as of February 2020 [2].

Research into Jupiter's trojan asteroids continues, with the particular focus on their origins reliant on an understanding of their orbit stability [3], [4]. This informs studies into their composition [5], as travel to these asteroids is considered for their potential in mineral mining [6] [7].

The purpose of this report is to use numerical simulation techniques to investigate the stability of orbits about these Lagrange points, demonstrating the asteroid oscillate about these points under small perturbations and quantifying the absolute distance of the asteroids from the Lagrange point (the wander) during their orbits. The impact of variation in planetary/solar mass on asteroid orbit stability will also be considered. *Signpost what is included in each section?*

2 Theoretical Background?

2.1 Lagrange Points

The asteroids exist at/near Lagrange points, defined in Lagrange's initial analysis of the three-body problem in 1772 [8], were he demonstrated the existence of five equilibrium points for an object of negligible mass orbiting under the gravitational effect of two larger masses. Three of these equilibrium points, L_1-L_3 lie on the line joining the two masses, while each of the remaining two points, L_4 and L_5, lie at the apex of an equilateral triangle with base equal to the separation of the two masses (see Figure 1). Despite all these points being potential maxima, stable motion is possible around L_4 and L_5 due to the Coriolis force [9].

Figure 1 depicts orbits about L_4 and L_5 (known as tadpole orbits), as well as orbits between Lagrange points are also possible (such as horseshoe orbits), described by Murray et al. [11].

This report will focus on tadpole orbits, a well documented feature of Trojan orbits [13], [14], and the restricted three-body problem in general. Their distinctive shape is result of a long-period motion about the equilibrium point combining with a short-period oscillation due to Keplerian motion of the asteroid.

Szebehely et al. [15] predict this short period tends to the planetary period in the small plan-
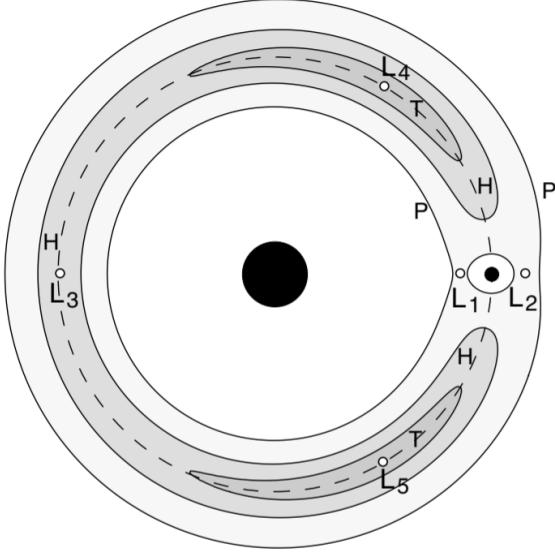
Figure 1: *The location of the five Lagrange equilibrium points in the circular-restricted three-body problem. The solar and planetary masses are denoted by the large and small filled circles, and the letters P, H, and T denote passing, horseshoe, and tadpole orbits respectively. Note that the two masses form an equilateral triangle with each of the L_4 and L_5 points. Reproduced from Marzari et al. [10]*

etary mass limit, while the long period is given by

$$T_{long} = T_P \sqrt{\frac{4}{27\mu_2}}, \quad (1)$$

where $\mu_2 = m_2/(m_1 + m_2)$ and T_P is the period of planetary orbit.

2.2 Theoretical Model

The three body problem, where the dynamics of three interacting bodies are determined given their initial positions and velocities, has no analytical (closed-form) solution in the general case [16].

In this report, I will consider the circular, restricted, three-body problem, where two of the bodies move in circular, coplanar orbits about their common centre of mass (CoM), unaffected by the negligible mass of the third body. I will also assume that all interactions are via Newtonian gravity.

The system of differential coordinates determine the position and velocity of the asteroids,

with two equations per spatial coordinate.

$$\frac{dr_i}{dt} = v_i, \frac{dv_i}{dt} = g_i, \quad i = x, y \quad (2)$$

In this, g_i is given by:

$$\mathbf{g} = -\frac{GM_s}{|\mathbf{r} - \mathbf{r}_s|^3}(\mathbf{r} - \mathbf{r}_s) - \frac{GM_p}{|\mathbf{r} - \mathbf{r}_p|^3}(\mathbf{r} - \mathbf{r}_p) \quad (3)$$

where the subscripts s and p refer to solar and planetary properties respectively.

We may also consider a frame rotating at the same speed as the massive bodies. As there is 1:1 orbital resonance between Jupiter and the asteroids, all three bodies are stationary in this frame. This significantly increases the accuracy of numerical simulations, as the exact solution is stationary with no explicit time dependence, rather then requiring an infinite power series [17], [18].

When transforming into this rotating non-inertial frame, g_i gains an additional virtual force term with coupling between the spatial coordinates. This is given below as the sum of the centripetal and Coriolis forces:

$$\Delta g_i = \Omega^2 r_i - 2[\mathbf{\Omega} \times \mathbf{v}]_i \quad (4)$$

where Ω is the angular speed of the rotating frame, and $\mathbf{v}$ is the velocity of the asteroid within this frame.

2.3 Symmetry

This problem contains a number of symmetries, which could be employed to simplify the problem and reduce the computational load. The Trojan and Greek asteroids are in equivalent positions, so experience the same forces, and the system is rotationally and inversion symmetric, so the choice of initial point and orbit direction is arbitrary. Therefore only the Greeks, orbiting counter-clockwise with perturbations applied at t = 0, need to be investigated.

2.4 Orbit Geometry

As the three bodies considered here form an equilateral triangle in the initial equilibrium state, as depicted in Figure 2, we can derive the polar coordinates of each body with respect to the centre of mass about which the bodies orbit.

Using standard trigonometric relations, it is simple to show that the values r_a and θ are given by:
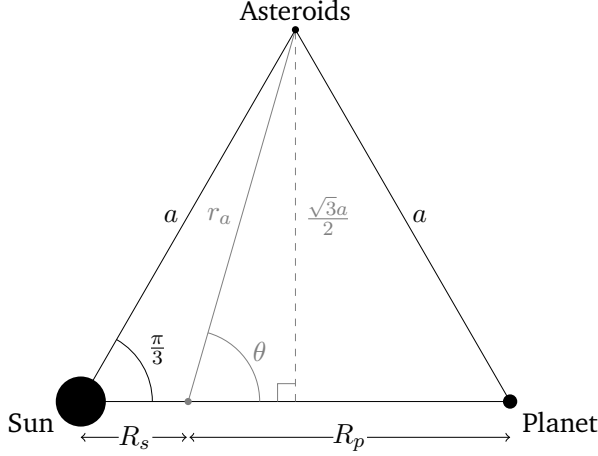
Figure 2: *A geometric depiction of the three-body system, in the case where the planet has a mass equal to a third of the sun, and asteroids are considered at the L_4 point. R_s and R_p denote the (fixed) radii from the centre of mass (the grey point) to the Sun and the planet respectively, while r_a denotes the radius of the asteroids.*

$$r_a = \sqrt{a^2 + R_s R_p}, \quad \theta = \tan^{-1}\left(\frac{a\sin\left(\frac{\pi}{3}\right)}{R_p - \frac{a}{2}}\right) \quad (5)$$

Furthermore, the Lagrange point in Cartesian coordinates based about the CoM is easily found to be:

$$(x, y) = \left(R_p - \frac{a}{2}, \frac{\sqrt{3}a}{2}\right) \quad (6)$$

Finally, equating the gravitational and centripetal forces on the planet allows the derivation of its (and all other bodies') orbital velocity:

$$\Omega = \sqrt{\frac{G(M_s + M_p)}{a^3}} \quad (7)$$

3 Methodology

This system of coupled first-order ordinary differential equations (ODEs) was solved using the scipy solve_ivp function. The time span was taken as 100 orbits (with 100 points sampled per orbit) unless otherwise stated; this corresponds to 1185 Earth years. Rescaled solar system units are used for mathematical ease, so distances are measured in astronomical units (AU), time in earth years and mass in multiples of the solar mass, and to prevent floating point overflows due to the magnitude of the quantities considered in SI units.

The wander was defined as the maximum distance of the asteroid from the initial point during the orbit (for small perturbations this is also approximately the separation from the Lagrange point). Initial conditions are defined by the Lagrange point in each frame, with the initial velocity in the stationary frame defined by the period of Jupiter's orbit, and split into Cartesian components.

3.1 Integration Method

Within solve_ivp, the default solver is RK45 (an explicit Runge-Kutta method of order 5(4) [19]) and gives a deviation in asteroid position (from the Lagrange point) in the order of 10^{-4} AU in the rotating frame over 50 years. This is larger than expected, indicating the system of equations requires an unreasonably small step size for numerical stability with respect to this method, even in regions where the solution curve is smooth [20]. This suggests the system is stiff, and solvers designed for this typically do more work per step, allowing them to take much larger steps, and have improved numerical stability compared to the non-stiff solvers such as RK45 [21].

Instead the stiff "Radau" solver (an implicit Runge-Kutta method of the Radau IIA family of order 5 [22]) is used for increased stability [23], and achieves a deviation in asteroid position in the order of 10^{-13} AU instead. This also ensures stability in the stationary frame, with deviations of 0.76% in asteroid separation from Jupiter over 10^3 years, compared to 53% for the best non-stiff solvers.

3.2 Programme Structure

Global constants such as solar mass, and sun–planet separation, along with derived values from these such as orbital period and solar radius from the CoM, are given in an importable python module "*constants*".

Functions to evaluate these coupled differential equation systems are defined in module "*orbits*", while additional functions to evaluate the wander during the orbit (under different sampling routines) are implemented in "*wander*". Further files then import these modules and produce the plots given in this report, fully detailed in appendix A.

To consider a varying planet mass, it was considered preferable to avoid reconstructing all func-

tions to take this as an argument as this requires re-evaluating all initial derived constants. Therefore, I iterate over alternative masses, re-defining constant values in this instance, and then directly import the required functions to compute the orbit. **REPHRASE?**

Complete code listings are given in appendix B.

3.3 Performance

Sampling 100 points per orbit for 100 orbits takes a mean time of 16.97 ± 34 ms, with sub-linear scaling for sampling rate and orbit number up to the array memory limit, achieved through the optimised integration routines within solve_ivp.

4 Results

4.1 Stability of Lagrange Points

Considering the Greeks' orbit without perturbations applied, it has a maximum deviation of 4.68×10^{-13} AU over 100 orbits (1185 years). This value is unchanged if 1000 orbits are considered instead, confirming the stability of this Lagrange point.

In the stationary frame, this wander from the (now moving) Lagrange point is depicted in Figure 3. The deviation oscillates with a magnitude of 9.10×10^{-2} AU, and a period of 148 ± 4 years, where the error was determined by the width of the Fourier peak. This is modulated with a faster oscillation component of 11.85 ± 0.27 years, equivalent to the orbital period of the asteroids.

These much more significant errors are due to time dependence in the exact solution, as detailed in Section 2.2. Energy can also be evaluated, and conserved, in this inertial frame; asteroid specific energy varies within only 0.113% of the initial value, and with a similar periodicity to wander. Energy is also negative, confirming the asteroids are located within a bound orbit.

Animations produced to demonstrate the orbit in the stationary frame are included in Supplementary Material I-II. Animation I depicts the orbit as evaluated by the radau solver, while II depicts it with LSODA, demonstrating the drift present over time with non-stiff solvers.
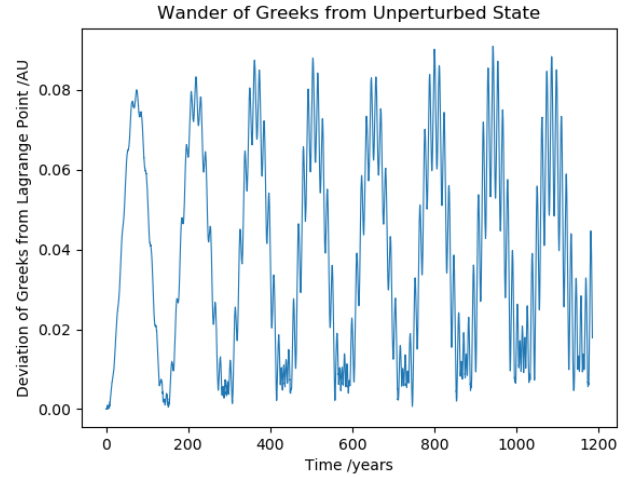

Figure 3: *The wander of Greek asteroids from the Lagrange point in the stationary frame. Note the two oscillation components and constant maximum oscillation amplitude over time, demonstrating this point is indeed stable.*

4.2 Wander Analysis

The wander from the initial point was calculated for random perturbations with a maximum magnitude of 1% of the displacement from the origin, and considered separately perturbation components parallel and perpendicular to the position vector from the CoM (hereafter referred to as radial and tangential components respectively). By considering these perturbations across position space, it was clear that the wander is fully determined by the radial component, with no tangential dependence (as shown in Figure 4).

Figure 4a demonstrates a polynomial dependence on perturbation size in the radial direction, with a negligible constant term. While a quadratic has been fitted here, it was not possible to eliminate the possibility of higher order terms, as increasing perturbation size beyond 0.06 AU can lead to unstable orbits.

We may consider the wander resulting from perturbations in position and velocity space. Figure 5a clearly shows the dependence on radial position perturbations only, while Figure 5b shows a similar the dependence on tangential velocity perturbations.
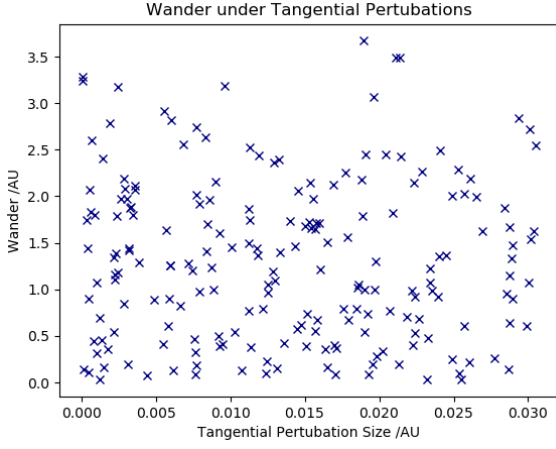
4.3 Orbit Types

Figure 6 displays orbits resulting from small perturbations in the radial and tangential directions.
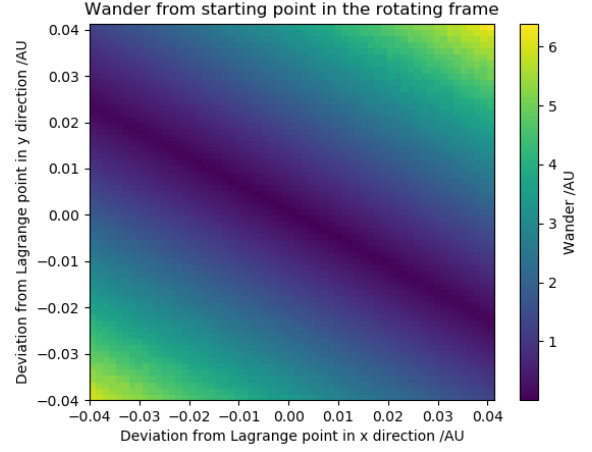
The "tadpole" orbit in Figure 6a consists of two
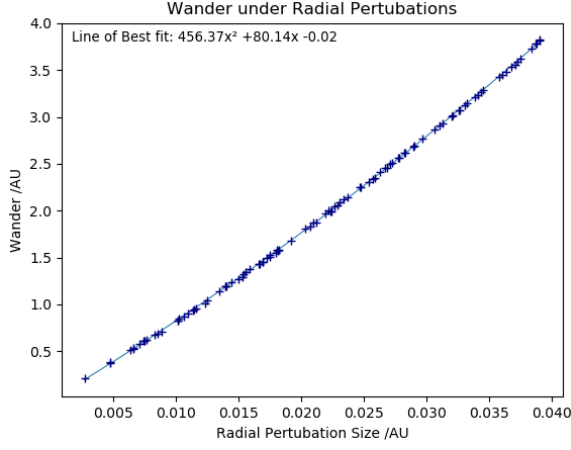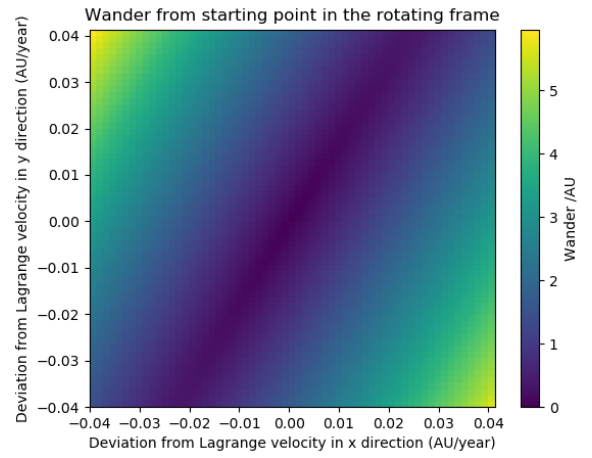
(a) *Radial*

(b) *Tangential*

Figure 4: *Wander from an initial perturbation with maximum relative magnitude of 0.1% of the displacement from the origin, given in radial and tangential directions.*

(a) *Position*

(b) *Velocity*

Figure 5: *Wander from an initial point in position and velocity space, only calculated over 50 orbits with 30 points per orbit to reduce computational load. Note the dependence on radial position and tangential velocity perturbation components.*

oscillating components, as described in Section 2.1. The short period, measured at 11.85 ± 0.61 years, is in agreement with planetary orbital period as expected; meanwhile the long period is measured to be 148 ± 5 years, in agreement with the analytical value of 144 years.

For a narrow range of larger perturbations, stable horseshoe orbits encompassing both Lagrange points may also be observed as depicted in Figure 7. This has a period of 29.9 years, in agreement with Taylor et al.'s numerical result of 30.2 ± 0.6 years [12].

4.4   Perturbations in z-direction

4.5   Variation of Planetary Mass

5   Discussion

6   Conclusion
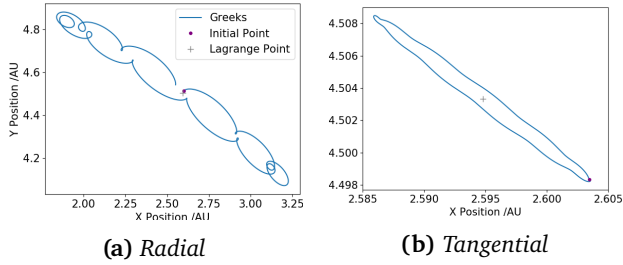
(a) *Radial*

(b) *Tangential*

Figure 6: *Orbits from an initial perturbation of magnitude 0.01 AU from the origin, in radial and tangential directions, over 12 orbital periods. Note the 'tadpole' features resulting from the radial perturbation, and the significantly larger wander than from the tangential perturbation.*
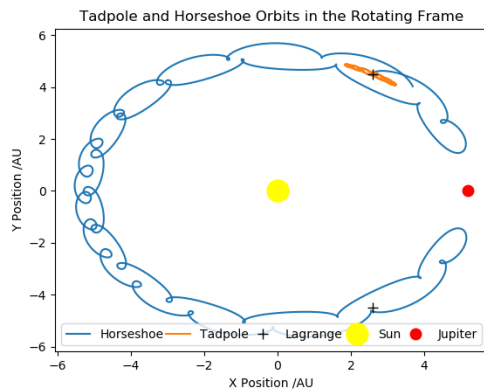

Figure 7: *Horseshoe and Tadpole orbits in the rotating frame, from radial perturbations of 0.07 and 0.01 AU respectively, over 30 orbital periods.*

References

[1]S. B. Nicholson, "The trojan asteroids", Leaflet of the Astronomical Society of the Pacific **8**, 239 (1961).

[2]Minor Planet Centre, International Astronomical Union, *Trojan minor planets*, (2020) `https://minorplanetcenter.net//iau/lists/Trojans.html`.

[3]R. P. D. Sisto, X. S. Ramos, and T. Gallardo, "The dynamical evolution of escaped jupiter trojan asteroids, link to other minor body populations", Icarus **319**, 828–839 (2019).

[4]D. Nesvorný, D. Vokrouhlický, W. F. Bottke, and H. F. Levison, "Evidence for very early migration of the solar system planets from the patroclus–menoetius binary jupiter trojan", Nature Astronomy **2**, 878–882 (2018).

[5]M. E. Brown, "The 3–4 micrometer spectra of jupiter trojan asteroids", The Astronomical Journal **152**, 159 (2016).

[6]T. Okada, T. Iwata, J. Matsumoto, J.-P. Bibring, S. Ulamec, R. Jaumann, R. Nakamura, H. Yano, Y. Kebukawa, J. Aoki, Y. Kawai, K. Terada, M. Toyoda, M. Ito, K. Yabuta, H. Yurimoto, Y. Saito, S. Yokota, C. Okamoto, S. Matsuura, K. Tsumura, D. Yonetoku, T. Mihara, A. Matsuoka, R. Nomura, T. Hirai, N. Grand, H. Cottin, L. Thirkell, C. Briois, T. Saiki, H. Kato, O. Mori, and J. Kawaguchi, "Science and exploration of a jupiter trojan asteroid in the solar-power sail mission", in 48th lunar and planetary science conference (Mar. 2017).

[7]H. F. Levison and Lucy Science Team, "Lucy: Surveying the Diversity of the Trojan Asteroids, the Fossils of Planet Formation", in Lunar and planetary science conference, Lunar and Planetary Science Conference (Mar. 2016), p. 2061.

[8]J.-L. Lagrange, "Essai sur le probléme des trois corps", Prix de l'Académie Royale des Sciences de Paris **IX** (1772).

[9]J. Lissauer and C. Murray, "Solar system dynamics: regular and chaotic motion", in *Encyclopedia of the solar system (third edition)* (2014).

[10]F. Marzari, H. Scholl, C. Murray, and C. Lagerkvist, "Origin and evolution of trojan asteroids", Asteroids III (2002).

[11]C. D. Murray and S. F. Dermott, *Solar system dynamics* (Cambridge University Press, 1999), pp. 95–102.

[12]D. B. Taylor, "Horseshoe periodic orbits in the restricted problem of three bodies for a sun-Jupiter mass ratio", Astronomy and Astrophysics **103**, 288–294 (1981).

[13]B. Garfinkel, "Theory of the trojan asteroids, iv", Celestial Mechanics **30**, 373–383 (1983).

[14]S. F. Dermott and C. Murray, "The dynamics of tadpole and horseshoe orbits", Icarus **48**, 1–11 (1981).

[15]V. Szebehely and E. Grebenikov, "Theory of orbits-the restricted problem of three bodies", Soviet Astronomy **13**, 364 (1969).

[16]J. Barrow Green, "The princeton companion to mathematics", in *The three-body problem*, edited by T. Gowers (Princetown University Press, 2008) Chap. V, pp. 726–728.

[17]N. Guglielmi and E. Hairer, "Implementing radau IIA methods for stiff delay differential equations", Computing **67**, 1–12 (2001).

[18]R. LeVeque, *Finite difference methods for ordinary and partial differential equations : steady-state and time-dependent problems* (Society for Industrial and Applied Mathematics, Philadelphia, PA, 2007), pp. 131–153.

[19]J. Dormand and P. Prince, "A family of embedded runge-kutta formulae", Journal of Computational and Applied Mathematics **6**, 19–26 (1980).

[20]J. D. Lambert, *Numerical methods for ordinary differential systems : the initial value problem* (Wiley, Chichester New York, 1991), pp. 217–220.

[21]G. D. Byrne and A. C. Hindmarsh, "Stiff ODE solvers: a review of current and coming attractions", Journal of Computational Physics **70**, 1–62 (1987).

[22]E. Hairer, *Solving ordinary differential equations II* (Springer, Berlin, 2010).

[23]R. Frank, J. Schneid, and C. W. Ueberhuber, "Stability properties of implicit runge–kutta methods", SIAM Journal on Numerical Analysis **22**, 497–514 (1985).

Appendix A Program Structure

Global constants, along with derived values from these are given in an python module "*constants*", from which relevant variable are imported in all other scripts.

Functions to evaluate these coupled differential equation systems are defined in module "*orbits*", while additional functions to evaluate the wander during the orbit are implemented in "*wander*". These modules are both imported into the scripts below for plotting and analysis, and given in the listings in Appendix B.

Wander from unperturbed initial conditions is calculated within "*lagrange_stability*", with ODE solver performance also evaluated here. Orbits in the stationary frame are animated and saved within "*stat_frame_video*".

2D perturbations are characterised in *perturbation_2D*.

Appendix B Code Listings

```python
import math
import numpy as np
from scipy import integrate
import matplotlib.pyplot as plt

from constants import G, M_S, M_P, R, ORBIT_NUM, PRECISION
# User defined constants
from constants import (
    solar_rad,
    planet_rad,
    period,
    omega,
    time_span,
)  # Derived constants
```